

Contaminant-Source Detection in a Water Distribution System Using the Ensemble Kalman Filter

Original

Contaminant-Source Detection in a Water Distribution System Using the Ensemble Kalman Filter / Butera, Ilaria; Jaime Gómez-Hernández, J.; Nicotra, Silvia. - In: JOURNAL OF WATER RESOURCES PLANNING AND MANAGEMENT. - ISSN 0733-9496. - STAMPA. - 147:7(2021). [10.1061/(ASCE)WR.1943-5452.0001383]

Availability:

This version is available at: 11583/2962390 since: 2022-05-02T15:17:26Z

Publisher:

ASCE

Published

DOI:10.1061/(ASCE)WR.1943-5452.0001383

Terms of use:

openAccess

This article is made available under terms and conditions as specified in the corresponding bibliographic description in the repository

Publisher copyright

ASCE postprint/Author's Accepted Manuscript

This material may be downloaded for personal use only. Any other use requires prior permission of the American Society of Civil Engineers. This material may be found at [http://dx.doi.org/10.1061/\(ASCE\)WR.1943-5452.0001383](http://dx.doi.org/10.1061/(ASCE)WR.1943-5452.0001383).

(Article begins on next page)

Contaminant-Source Detection in a Water Distribution System Using the Ensemble Kalman Filter

Ilaria Butera¹, J. Jaime Gómez-Hernández², and Silvia Nicotra³

¹Department of Environment, Land and Infrastructure Engineering, Politecnico di Torino. Italy.

Email: ilaria.butera@polito.it

²Institute for Water and Environmental Engineering. Universitat Politècnica de València. Spain.

Email: jgomez@upv.es

³Department of Environment, Land and Infrastructure Engineering, Politecnico di Torino. Italy.

Email: silvia.nicotra@polito.it

ABSTRACT

Early detection of a contamination leach into a water distribution system, followed by the identification of the source and an evaluation of the total amount of contaminant that has been injected into the system is of paramount importance in order to protect water user's health. The ensemble Kalman filter, which has been recently applied in hydrogeology to detect contaminant sources in aquifers, is extended to the identification of a contaminant source and its intensity in a water distribution system. The driving concept is the assimilation of contaminant observations at the nodes of the pipeline network at specified time intervals until enough information has been collected to allow the positioning of the source and the estimation of its intensity. Several scenarios are analyzed considering sources at different nodes, with different delays between the beginning of the pollution and the start of the measurements, with different sampling time intervals, and with different observation ending times. The scenarios are carried out in the bench-marking Anytown network demonstrating the ability of the ensemble Kalman filter for contaminant-source detection in real water distribution systems. The use of the ensemble Kalman filter supposed a major

breakthrough in the inverse modeling of subsurface flow and transport, the successful results of its application to the synthetic Anytown network warrant further exploration of its capabilities in the realm of water distribution systems.

INTRODUCTION

Water distribution systems (WDSs) are a key infrastructure for the preservation of people's health. Intentional or accidental contamination of the systems has to be detected in the shortest possible period to reduce damages, for which Early Warning Systems are desirable. To limit the damages caused by a contamination event, it is important to detect both the source location and the release intensity; the source location will allow repairing the system and preventing further contamination and the release intensity will allow estimating the amount of contaminant injected.

Measurement networks are being deployed in WDSs to detect the presence of pollutants and a large effort has been done to identify strategies for the optimal location of sensors (e.g., [Hart and Murray 2010](#); [Ung et al. 2017](#)). In the last fifteen years, an interest in using the observed concentration measurements at some nodes of the WDS to identify the source location and the release history has grown, and a number of methodologies has been developed; a good review paper on the subject was published by [Adedoja et al. \(2018\)](#). The authors of this review identify three types of approaches: probabilistic approaches, simulation approaches and others, like artificial neural networks ([Kim et al. 2008](#)) or hybrid methods ([Liu et al. 2012](#)). A few of the works discussed in the review are worth to be singled out: [Tryby et al. \(2010\)](#) propose an optimal sensor placement design for source identification using minimum least-squares optimization; [De Sanctis et al. \(2010\)](#) use a particle backtracking method to identify the nodes of a network that are coherent with the presence/absence of contamination at sensor locations; [Liu et al. \(2011\)](#) propose an adaptive dynamic optimization procedure for contaminant source identification aimed at avoiding the ill-posedness of the problem; [Eliades and Polycarpou \(2012\)](#) use decision trees to identify the network nodes where the contamination took place with as few manual samplings as possible; [Shen and McBean \(2012\)](#) identify potential intrusion nodes using parallel computing, a large database, and data-mining; [Wang and Harrison \(2013\)](#) implement Markov chain Monte Carlo for

51 contaminant source identification, although they recognize that further improvements are needed
52 to make the approach operational; [Perelman and Ostfeld \(2013\)](#) use Bayesian networks to estimate
53 the likelihood of the injection location of a contaminant and its propagation into the system; [Butera
54 et al. \(2013a\)](#) use a geostatistical approach to recover the release history of a pollutant intrusion;
55 [Yang and Boccelli \(2014\)](#) mix a Bayesian approach with backtracking to calculate the probabilities
56 of potential source locations; [Wang and Harrison \(2014\)](#) mix a Bayesian approach with support
57 vector machines to improve the likelihood calculations; [Seth et al. \(2016\)](#) propose a systematic
58 procedure for testing and evaluating source identification methods; and [Ung et al. \(2017\)](#) couple an
59 adjoint source identification method and a Monte Carlo sensor placement algorithm to optimally
60 and accurately place sensors. The broad review by [\(Adedoja et al. 2018\)](#) highlights the current
61 relevance of the research topic and concludes that more effort is necessary to make these models
62 applicable in real life.

63 From a mathematical point of view, identifying a contaminant source from some concentration
64 data can be cast as an inverse problem: information about the state of the system is used to identify
65 parameters, boundary conditions or forcing terms of the system, which is modeled by a system
66 state equation. Inverse problems have been addressed for many years in hydrology and hydraulics
67 with both deterministic and stochastic approaches. A good review of inverse models in subsurface
68 hydrology can be found in [Zhou et al. \(2014\)](#), and some applications in surface hydrology in [D’Oria
69 et al. \(2014\)](#), [D’Oria et al. \(2017\)](#) or [Todaro et al. \(2019\)](#). Probably, subsurface hydrology has been
70 the area with the largest body of research in the subject, from the early deterministic works (i.e.,
71 [de Marsily et al. 1984](#); [Carrera and Neuman 1986](#)) to the later stochastic ones (i.e, [Woodbury
72 and Ulrych 1993](#); [Wen et al. 1999](#); [Li et al. 2012](#); [Capilla et al. 1999](#); [Sun et al. 2009](#); [Zhou
73 et al. 2012](#)). In the last decades, the use of the ensemble Kalman filter has gained much attention
74 as an inverse modeling method, even though in its inception it was not considered an inverse
75 model but a filtering algorithm to filter out model and observation error from model predictions.
76 Applications in hydrogeology (i.e., [Franssen and Kinzelbach 2009](#); [Schöniger et al. 2012](#); [Zhou
77 et al. 2012](#); [Xu et al. 2013](#)) and in petroleum engineering (ie., [Wen et al. 1999](#); [Chen et al. 2010](#))

78 are abundant. Implementations of inverse modeling for the identification of contaminant sources
79 in groundwater can be found in the reviews by [Atmadja and Bagtzoglou \(2001\)](#), [Bagtzoglou and](#)
80 [Atmadja \(2005\)](#), [Michalak and Kitanidis \(2004\)](#) or [Sun et al. \(2006\)](#). More recent approaches have
81 used methods based on minimum relative entropy, the geostatistical approach or the use of adjoint
82 states ([Bagtzoglou et al. 1992](#); [Butera et al. 2013b](#); [Koch and Nowak 2016](#); [Neupauer and Wilson](#)
83 [1999](#); [Woodbury and Ulrych 1996](#)).

84 Aquifers and WDS are conceptually similar, in both cases water (and solutes) move in a
85 heterogeneous media, driven mainly by gravity and pumping that induce changes in water pressures
86 and solute concentrations in space and time. In both systems, there is a state equation that permits
87 the prediction of the system state at time t , given the state at time $t - \Delta t$; a state equation that depends
88 on geometrical and material parameters, such as aquifer extension and hydraulic conductivities (in
89 aquifers), or pipe lengths and roughness coefficients (in WDS). These similarities suggested that
90 an algorithm such as the The main difference is that the aquifer state is defined continuously in
91 two-dimensional or three-dimensional space, but WDS state is defined continuously in a number of
92 one-dimensional segments. This difference will require a special treatment as explained later. This
93 similarity has encouraged some researchers to use approaches that have worked in hydrogeology
94 in WDS. For example, the work by ([Butera et al. 2013a](#)) demonstrates the application of the
95 geostatistical approach for the identification of the release history of a contamination event in a
96 WDS. The motivation of this paper is to demonstrate the application of the ensemble Kalman filter,
97 a technique that recently has demonstrated its potential in groundwater modeling for the purpose
98 of contaminant-source identification ([Chen et al. 2018](#); [Xu and Gómez-Hernández 2016](#); [Xu and](#)
99 [Gómez-Hernández 2018](#)) to the field of WDS. The ensemble Kalman filter has already been used
100 in WDSs, for instance, ([Rajakumar et al. 2019](#)) applied it to model the uncertainty on chlorine
101 concentration or ([Ye and Fenner 2014](#)) used it to detect bursts in WDSs, but, to the best of our
102 knowledge, it has not been applied to the problem of contaminant source and release identification.
103 This paper does benchmark the ensemble Kalman filter against other approaches developed for the
104 same purpose; it shows the potential of a new approach for source identification that is general,

105 simple to understand and implement, and that has proven its effectiveness in other fields. The
106 remainder of this manuscript is organized as follows: a brief description of the ensemble Kalman
107 filter is presented, followed by a description of the case study and finalizing with a discussion of
108 the results and some conclusions.

109 **THE ENSEMBLE KALMAN FILTER**

110 The ensemble Kalman filter (EnKF) was developed by Evensen (1994, 2003) to overcome the
111 difficulties of the Kalman filter to deal with systems that evolve non-linearly in space-time. Although
112 the filter was originally designed to improve the estimation of the state of the system, it has been
113 extended for the estimation of the parameters controlling the state equation, by considering these
114 parameters as state variables as part of what is called an augmented state. The resulting filter with
115 augmented state is a powerful inverse modeling algorithm. The main idea of the filtering algorithm
116 is the sequential forecasting and updating of the augmented state vector, in which the forecasting is
117 based on the state equation, and the updating is based on the discrepancy between observations and
118 predictions to modify the augmented state. This forecast and update steps are repeated each time
119 that a new sets of observations is available. The forecast can be done with regard to the last update
120 of the state variables and using the last update of the system parameters, or it can be done with
121 the state variables from time zero and the last update of the system parameters, in cases in which
122 the update of the state may results in a state spatial distribution that may violate some fundamental
123 laws, such as mass conservation, or, as it will be in this case, the updated parameters modify the
124 way the system would have behaved since time zero. Indeed, in the problem of contaminant source
125 identification, updating the position of the source can only be accounted for to predict the state in
126 the next time step by rerunning the forecast from time zero, when the source enters the system. For
127 this reason, this approach is referred to as the restart ensemble Kalman filter (rEnKF). In this paper,
128 the state variables are solute concentrations and the model parameters to be inverted are the node at
129 which the solute enters the WDS and the release intensity. Let \mathbf{X} be the vector of parameters, and
130 \mathbf{Y} the vector of solute concentrations in the system. They both are related through a state equation

131 with given boundary, initial conditions and forcing terms,

$$132 \quad \mathbf{Y}(t) = \psi(\mathbf{X}, \mathbf{Y}(t - \Delta t)), \quad (1)$$

133 where t indicates time. In general, the state at time t is computed as a function of the state in the
134 previous time step $t - \Delta t$. In the rEnKF with augmented state, the state equation is rewritten as

$$135 \quad \begin{pmatrix} \mathbf{X}(t) \\ \mathbf{Y}(t) \end{pmatrix} = \begin{pmatrix} \mathbf{X}(t - \Delta t) \\ \psi(\mathbf{X}(t - \Delta t), \mathbf{Y}(0)) \end{pmatrix}. \quad (2)$$

136 The first step in the rEnKF is the forecast of the (augmented) system state for the next time step. This
137 forecast is performed using the state equation (2), on one hand we forecast the parameters, which
138 remain the same since we have no state equation for its evolution in time, on the other hand we
139 also forecast the state from time zero, this forecast will use the last update of the parameter values,
140 which will be performed in the assimilation step. At time zero, we assume that the contaminant
141 has not entered the system yet and therefore all values of $\mathbf{Y}(0)$ are equal to zero. The second
142 step is the updating of the augmented state once new observations are available. In this specific
143 implementation in which the forecast is always made from the state values at time zero, the interest
144 is in the update of the parameter values, since the updated states will be of no use for the next
145 forecast step. Given a set of state observations $\mathbf{Y}^{obs}(t)$, the discrepancy between forecast values
146 and observed ones will be used to update the parameter forecast in (2)

$$147 \quad \mathbf{X}^a(t) = \mathbf{X}(t) + \mathbf{G}(t) \left(\mathbf{Y}^{obs}(t) + \mathbf{e}(t) - \mathbf{Y}(t) \right), \quad (3)$$

148 where $\mathbf{X}^a(t)$ is the updated parameters values after data assimilation, $\mathbf{e}(t)$ is the observation error
149 with zero mean and covariance given by the matrix $\mathbf{R}(t)$, and $\mathbf{G}(t)$ is the Kalman gain, given by

$$150 \quad \mathbf{G}(t) = \mathbf{C}_{XY}(t) (\mathbf{C}_{YY}(t) + \mathbf{R}(t))^{-1}, \quad (4)$$

151 where $\mathbf{C}_{XY}(t)$ is the covariance between all the parameters and the state variables at observation
 152 locations, and $\mathbf{C}_{YY}(t)$ is the covariance of the state variable at observation locations. Therefore, if
 153 there are n_p parameters and n_o observations locations, vectors $\mathbf{X}^a(t)$ and $\mathbf{X}(t)$ have sizes $n_p \times 1$,
 154 vectors $\mathbf{Y}^{obs}(t)$, $\mathbf{e}(t)$ and $\mathbf{Y}(t)$ have sizes $n_o \times 1$, the Kalman gain $\mathbf{G}(t)$ is a matrix of size $n_p \times n_o$,
 155 the covariance \mathbf{C}_{XY} is a matrix of size $n_p \times n_o$, and the matrices $\mathbf{C}_{YY}(t)$ and $\mathbf{R}(t)$ are of size $n_o \times n_o$,
 156 with the matrix $\mathbf{R}(t)$ generally being a diagonal matrix when the observation errors are modeled as
 157 uncorrelated. The Kalman gain is a unique matrix that is computed after each observation step and
 158 used to update all realizations.

159 In the earlier versions of the Kalman filter and the extended Kalman filter, the covariance
 160 matrices were computed using the state equation. Such a computation is exact if the state equation
 161 is linear, but it is only approximate if it is not linear. The ensemble Kalman filter solves the problem
 162 of computing the covariances for non-linear state transition equations. In the EnKF formulation,
 163 the covariances in Eq. (4) are estimated from an ensemble of realizations of parameters and state
 164 variables (calculated according to the state equation) in which each realization goes through the
 165 two steps of forecast and update described above. It is after the forecast step that the covariances
 166 matrices are calculated; specifically, the two covariances involved in the computation of the Kalman
 167 gain are estimated from a set of N ensemble realizations as

$$168 \quad \mathbf{C}_{XY}(t) = \frac{1}{N-1} \left((\overline{\overline{\mathbf{X}}} - \overline{\overline{\mathbf{X}}}\mathbf{1}_{1 \times N})(\overline{\overline{\mathbf{Y}}} - \overline{\overline{\mathbf{Y}}}\mathbf{1}_{1 \times N})^T \right), \quad (5)$$

$$169 \quad \mathbf{C}_{YY}(t) = \frac{1}{N-1} \left((\overline{\overline{\mathbf{Y}}} - \overline{\overline{\mathbf{Y}}}\mathbf{1}_{1 \times N})(\overline{\overline{\mathbf{Y}}} - \overline{\overline{\mathbf{Y}}}\mathbf{1}_{1 \times N})^T \right), \quad (6)$$

170 where $\mathbf{1}_{1 \times N}$ represents a row vector with N ones, $\overline{\overline{\mathbf{X}}}$ is a matrix of size $n_p \times N$ in which each column
 171 contains the parameters values of a realization, $\overline{\overline{\mathbf{X}}}$ is a column vector of size $n_p \times 1$ with the average
 172 values of each parameter computed through the realizations $\overline{\overline{\mathbf{X}}} = \frac{1}{N}\overline{\overline{\mathbf{X}}}\mathbf{1}_{N \times 1}$ (now $\mathbf{1}_{N \times 1}$ is a column
 173 vector with N ones), and, similarly, $\overline{\overline{\mathbf{Y}}}$ is a matrix of size $n_o \times N$ in which each column contains the
 174 forecast concentrations at observation locations, and $\overline{\overline{\mathbf{Y}}}$ is a column vector of size $n_o \times 1$ with the
 175 average state values at each observation location computed through the ensemble of realizations

$$\bar{\mathbf{Y}} = \frac{1}{N}(\bar{\mathbf{Y}}\mathbf{1}_{N \times 1}).$$

The restart ensemble Kalman filter workflow is as follows:

1. Set the initial state of the system $\bar{\mathbf{Y}}(0)$, and generate an initial ensemble of N realizations of the parameters to be identified $\bar{\mathbf{X}}(0)$ then, repeat the following steps for as many time steps as observations are available.
2. For each realization, forecast the state of the system to the next time step for which observations are available using Eq. (2). In this case, a solute transport model is used for the forecast.
3. Extract the forecast values at observed locations from all realizations, build matrices $\bar{\mathbf{X}}$ and $\bar{\mathbf{Y}}$, and compute the covariances in Eqs. (5) and (6)
4. Compute the Kalman gain in Eq. (4).
5. For each realization, update the parameter values using Eq. (3).
6. Go back to 2 while new observations are sampled.

The ensemble of realizations provides a set of values for each parameter, which will converge to a final set of ensemble values the mean of which should be close to the actual parameter value and the variance of which gives an estimate of the uncertainty about the estimation. At time zero, the mean and variance of the parameters are those of the random functions used to generate them at step 1 of the workflow; then, the ensembles of updated parameters should narrow their variability and converge towards the underlying values. The main problem of the ensemble Kalman filter occurs when the ensemble of realizations collapses onto a single value which is far from the actual value (i.e., [Xu et al. 2013](#)). This is referred to as filter collapsing, or filter inbreeding and it is generally related to an underestimation of the covariance in Eqs. (6) and (5).

In the present application, the algorithm will be used for the identification of three parameters, the two spatial coordinates of the source and the logarithm of the release intensity of the contamination injected into the system. The use of the logarithm of the intensity is because the updating equation (3) does not preclude the updated values to be negative, while working with logarithms,

202 positive release intensities will be ensured.

203 **CASE STUDY**

204 This is an academic exercise in the absence of real data. It is intended to solve a set of different
205 scenarios, each with a predefined source location and intensity. To expand the casuistry, up to 16
206 different scenarios will be considered, with the source located in each case at a different node in the
207 network, and for all of them an intensity of 100 mg/l will be assumed. As in this case the location
208 of the source is known in advance for each scenario, the goal is that the evolution of the $\mathbf{X}^a(t)$, as
209 new measurements are assimilated at each step, leads to the predefined location and intensity of the
210 source considered for each scenario. In a real case, such location and intensity will not be known in
211 advance, in such a case, the prediction will be given by the average of the ensemble of realizations
212 and the prediction uncertainty by their standard deviation.

213 The application of the rEnKF for the identification of the location and intensity of a contaminant
214 release into a WDS is applied to the Anytown network of [Walski et al. \(1987\)](#), a common benchmark
215 in water supply analysis. The Anytown network is composed of 16 nodes (not sequentially
216 numbered) and 32 links of lengths varying between 1828.8 m and 3657.7 m, which is sketched in
217 Fig. 1a. Water is supplied from groundwater resources through a pumping system into two storage
218 tanks. The daily mean discharge supplied by the network is equal to 365 l s^{-1} . Hourly patterns are
219 used to simulate a time variable demand, with values that go from 325 l s^{-1} to 475 l s^{-1} . Pipeline
220 roughness is described using a Hazen-Williams C-factor, which varies between 70 and 120.

221 A contaminant release of uniform intensity occurs in one of the 16 nodes of the system. The
222 release intensity, i , and the spatial coordinates of the source (x, y) are the three parameters to identify
223 by the rEnKF. The contaminant is a non-reactive solute; however, the proposed methodology could
224 be applied to reactive solutes simply modifying the state equation to account for the reactions.
225 The contaminant enters the system as a single source; the problem of multiple sources or varying
226 intensity sources has not been considered in this manuscript but deserves further consideration.
227 The software used to simulate the flow and transport in the pipe network is version 2.2 of EPANET
228 [Rossman 2000](#).

229 The simulation of the contaminant evolution in the perfectly known Anytown system is sampled
 230 at all nodes at specified times. These samples will be the observations against which the forecasted
 231 values during the application of the EnKF will be contrasted.

232 Contaminant sensors are located in all 16 nodes of the network. These sensors are activated
 233 at certain time t_1 after the release happens and measure the concentration at time increments Δt .
 234 They stop measuring after a certain t_{max} . In the following, a number of scenarios will be run to
 235 try to analyze the impact of t_1 . The meaning of t_1 is associated to the idea that the sensors are not
 236 continuously running at all times, and that they only start measuring after some warning is received
 237 and then an operator activates them. This activation could be immediate or it can be later, once
 238 the contaminant has already spread through the pipeline system. The scenarios will analyze also
 239 the impact of the sampling interval size, Δt ; and the impact of the magnitude of t_{max} , the time at
 240 which the system stops measuring, a small value of it will replicate a possible rupture of the sensor
 241 system.

242 The rEnKF starts with an ensemble of realizations for the three parameters. The number of
 243 realizations was initially 100 but it was reduced down to 48 when it was found that similar results
 244 were found with this smaller number. The initial set of coordinates for the 48 realizations is fixed
 245 and the same for all scenarios and realizations. It is shown in Fig. 1c. Notice that the source initial
 246 locations coincide with all nodes of the system plus the center point of all pipes. The initial set of
 247 release intensities is distributed uniformly in $[0.5I_1, 2I_1]$, where I_1 is the release intensity estimated
 248 at time t_1 when the sensors perform the first observation of concentrations and fluxes at all 16 nodes
 249 and given by:

$$250 \quad I_1 = \sum_{i=1}^{16} C_i(t_1)Q_i(t_1). \quad (7)$$

251 Measurement errors are modeled with a zero mean and a diagonal covariance matrix, $\mathbf{R} = \sigma_e^2 \mathcal{I}$,
 252 with $\sigma_e^2 = 10^{-5} \text{ mg}^2 \text{ l}^{-2}$, with \mathcal{I} being the identity matrix. This small measurement error variance
 253 is coherent with the concentrations observed in the network, which vary between 0 and 0.05 mg
 254 l^{-1} . (Although the injection load is of 100 mg l^{-1} , the contaminant gets quickly diluted and the

255 concentrations diminish very quickly.)

256 During the forecast step, if the concentrations modeled were below 10^{-6} mg l⁻¹, the concentra-
257 tion was set to zero to mimic the detection limit of the sensors.

258 During the forecast step, model uncertainties are introduced by adding an error to the base
259 demand at each node from a distribution of zero mean and standard deviation equal to 5% of the
260 base demand value.

261 During the updating step of the rEnKF, the coordinates of the source will be updated to some
262 values in the XY plane that will not necessarily fall on the pipeline system; for this reason, the
263 updated coordinate values resulting from the application of Eq. (3) to all the realizations are
264 relocated to the closest node on the discretized pipeline system shown in Fig. 1b.

265 During the updating step and in order to prevent filter collapsing, it is convenient to inflate the
266 covariance matrix, C_{YY} . After some tests, it was found that multiplying the diagonal of C_{YY} by 1.1
267 gives stable results.

268 **RESULTS AND DISCUSSION**

269 As already mentioned, a preliminary analysis was performed to decide on the size of the
270 ensemble and it was found that an ensemble of 48 realizations gave as good results as an ensemble
271 of 100 realizations, so it was decided to perform all analyses with $N = 48$.

272 In total, 16 scenarios have been considered with varying source locations, sensor start time
273 after release, maximum monitoring time, and interval between measurements. The combinations
274 of these values for each scenario are shown in Table 1.

275 In order to quantify the performance of the rEnKF in each scenario, four indicators are built.
276 The first one measures the lack of precision or the spread of the ensemble of coordinate realizations
277 at the end of the assimilation process by computing the square root of the moment of inertia of
278 these coordinates with respect to their center of mass. The second one measures the bias or the
279 lack of accuracy of the final ensemble of coordinate realizations by computing the square root of
280 the moment of inertia of these coordinates with respect to the true source location. In both cases,
281 these values are normalized by the corresponding values computed with the coordinate realizations

282 at time zero. Similarly, to evaluate the uncertainty of the release intensities at the end of the
 283 assimilation process, its coefficient of variation is computed, and to evaluate their bias the square
 284 root of the average square deviation between the ensemble intensities and the true one is computed
 285 and normalized by the true release intensity. These indicators have the following expressions

$$286 \quad i_1(t) = \sqrt{\frac{\sum_{j=1}^N d_j^2(t)}{\sum_{j=1}^N d_j^2(0)}}, \quad (8)$$

$$287 \quad i_2(t) = \sqrt{\frac{\sum_{j=1}^N s_j^2(t)}{\sum_{j=1}^N s_j^2(0)}}, \quad (9)$$

$$288 \quad i_3(t) = \frac{\sigma_I}{\bar{I}}, \quad (10)$$

$$289 \quad i_4(t) = \frac{\sqrt{\frac{1}{N} \sum_{j=1}^N (I_j - I_s)^2}}{I_s}, \quad (11)$$

290 where N is the number of realizations of the ensemble, $\{d_j, j = 1, \dots, N\}$ are the distances between
 291 each realization position and their center of mass, $\{s_j, j = 1, \dots, N\}$ are the distances between
 292 the each realization position and the true release location, $\{I_j, j = 1, \dots, N\}$ are the ensemble
 293 intensities, σ_I is the standard deviation of this ensemble, \bar{I} is the mean of this ensemble, and I_s is
 294 the true release intensity. Notice that these indicators are computed at the end of each assimilation
 295 step and their evolution in time measure the speed of convergence of the algorithm.

296 These indicators can be calculated in this case since this is an academic exercise. In a real
 297 situation, only indicators i_1 and i_3 could be computed and the success of the approach would be
 298 measured by the effective identification of the source.

299 The values of the four indicators together with the average distance between the ensemble of
 300 coordinate realizations and the true source location and the average difference between the ensemble
 301 of source intensities and the true one are shown in Table 2.

302 First thing to notice is that, for scenarios S1 and S7 the identification of the source coordinates
 303 is perfect, in both cases the sensor sampling starts late and the sampling interval is short. Fig 2
 304 shows a histogram of i_1 and i_2 computed at the end of the sampling for all scenarios, recall that

305 they measure, respectively, the intrinsic spread of the ensemble of source positions and the bias
306 with respect to the true value relative to the spread and bias of the initial source locations of Fig 1c.
307 For all cases, the spread measured by i_1 is reduced drastically to below 4% of the initial value, but
308 the bias measured by i_2 is kept at relatively larger values for a number of scenarios. The large bias
309 in scenario 8 (source at node 11) may be explained by the late start of the sensors, the biases for
310 scenarios 15 (source at 18) and 16 (source at 19) may be explained by the complex flow patterns
311 through these nodes linking several pipes. However, overall, the estimation of the source locations
312 is good to very good for all cases since the average deviation of the final positions from the true
313 locations are, for all cases, below 150 m, a small value compared with the pipe lengths, which range
314 between 1828 m and 3568 m.

315 Fig. 3 shows a histogram of i_3 and i_4 computed at the end of the sampling for all scenarios. The
316 spreads and the biases are always reduced below 10% of their initial values and for some scenarios
317 below 2%. The average difference between the final ensemble of intensities and the true value is
318 always small, less than $\pm 7 \text{ mg l}^{-1}$, except for S13. These results are indicative of a very good
319 identification of the release intensity. The worst estimates occur for scenarios 5, 6, 12, 13 and 16.
320 Scenarios 5 and 6 could be explained by a late start of the sampling process and the location of the
321 sources along the edge of the network (sources at nodes 8 and 9, respectively) but the behavior of
322 12, 13 and 16 is more difficult to explain (although it is worth to point out that, for these cases, the
323 source nodes, 15, 16 and 19, are linked by three pipes in the center of the network).

324 Fig. 4 shows the time evolution of i_1 and i_2 for case 6 (source at node 9) with a late start of the
325 sampling and a long sampling interval; this figure also shows the positions of the source location
326 realizations at $t_{max} = 600 \text{ min}$. It is interesting to see how, after a few samples, both i_1 and i_2 are
327 down to their minimum values, and how the final source location realizations are all very close to
328 or at the true source locations. Similar results are shown in Fig. 5 for scenario 12 with a release
329 from node 15. This scenario was not one of the best performers in terms of the indicators, yet, even
330 if the final set of realizations is biased with respect to the true source, the final estimate is close to
331 the true source.

332 Fig. 6 shows the time evolution of i_3 and i_4 for scenarios 6 and 12 that differ in the starting time
333 of the sampling. The most noticeable item is the large spread and bias of the updated intensities
334 during the first time steps and the sharp decrease of them as more concentrations are assimilated.
335 It also shows that starting the sampling as early as possible can help in identifying the release
336 intensity quickly.

337 In general, it can be concluded that an early detection of the release (i.e., activating the sensors
338 60 minutes after the release) followed by a continued sampling at a low frequency (i.e., every 30
339 minutes) is preferable than a late detection (i.e., activating the sensors 180 minutes after the release)
340 followed by a high-frequency sampling (i.e., every 10 minutes).

341 Finally, to illustrate the updating process of the source locations, the time evolution of the
342 ensemble of locations for scenarios 7 and 10 (release nodes 10 and 13, respectively) is shown in
343 Figs. 7 and 8, respectively. It is interesting to see how the source locations are being updated after
344 each observation to positions closer and closer to the true source until all ensemble converges onto
345 it.

346 The AnyTown network may be considered a simple network compared to a real network that
347 could have up to 10,000 nodes for 100,000 inhabitants. The simple case was chosen to test a new
348 approach that had never been tested in water distribution systems. Given its satisfactory results,
349 and considering that in hydrogeology, the EnKF has been applied to numerical models with tens
350 of thousands of discretizing elements, the method should also work in larger systems, with larger
351 computational times.

352 CONCLUSIONS

353 This work proposes an application of the restart ensemble Kalman filter (rEnKF) to the identi-
354 fication of the source location and intensity of a contaminant release in a water distribution system.
355 The method proposed has been tested in the Anytown network assuming a constant contaminant
356 injection. Contaminant observations at the nodes of the network are made with varying sampling
357 intervals and sampling start times since the release began. The exercise also considered a small
358 sampling error and errors in the estimation of the demand at each node. Sixteen scenarios were

359 analyzed in order to reproduce different measurement schemes. From the analysis it is concluded
360 that is best to detect the contamination as soon as possible, followed by a not necessarily very
361 high measurement frequency, for, after a few sampling steps, identify the source location and the
362 release intensity of the contamination release. Despite the small number of ensemble members
363 (only 48) the method proved to successfully identify the source location and release intensity. It
364 is concluded that the rEnKF is a valuable technique for source identification in water distribution
365 systems. Future research should include more realistic cases, with smaller number of sensors,
366 releases occurring anywhere in the network, non uniform releases, and larger sampling errors and
367 modeling errors. Other avenues of research should explore the simultaneous identification of the
368 source and the roughness coefficients of the pipes, in a manner similar how hydraulic conductivities
369 and contaminant source parameters are identified in aquifer applications.

370 **DATA AVAILABILITY**

371 All data, models, or code that support the findings of this study are available from the corre-
372 sponding author upon reasonable request.

373 **REFERENCES**

374 Adedaja, O. S., Hamam, Y., Khalaf, B., and Sadiku, R. (2018). “Towards development of an
375 optimization model to identify contamination source in a water distribution network.” *Water*,
376 10(5), 579.

377 Atmadja, J. and Bagtzoglou, A. C. (2001). “State of the Art Report on Mathematical Methods for
378 Groundwater Pollution Source Identification.” *Environmental Forensics*, 2(3), 205–214.

379 Bagtzoglou, A. C. and Atmadja, J. (2005). “Mathematical Methods for Hydrologic Inversion: The
380 Case of Pollution Source Identification.” *Water Pollution*, 5, 65–96.

381 Bagtzoglou, A. C., Dougherty, D. E., and Tompson, A. F. B. (1992). “Application of particle meth-
382 ods to reliable identification of groundwater pollution sources.” *Water Resources Management*,
383 6(1), 15–23.

384 Butera, I., Boano, F., Revelli, R., and Ridolfi, L. (2013a). “Recovering the release history of a

385 pollutant intrusion into a water supply system through a geostatistical approach.” *Journal of*
386 *Water Resources Planning and Management*, 139(4), 418–425.

387 Butera, I., Tanda, M. G., and Zanini, A. (2013b). “Simultaneous identification of the pollutant
388 release history and the source location in groundwater by means of a geostatistical approach.”
389 *Stochastic Environmental Research and Risk Assessment*, 27(5), 1269–1280.

390 Capilla, J. E., Rodrigo, J., and Gómez-Hernández, J. J. (1999). “Simulation of non-gaussian
391 transmissivity fields honoring piezometric data and integrating soft and secondary information.”
392 *Mathematical Geology*, 31(7), 907–927.

393 Carrera, J. and Neuman, S. P. (1986). “Estimation of aquifer parameters under transient and
394 steady state conditions: 1. maximum likelihood method incorporating prior information.” *Water*
395 *Resources Research*, 22(2), 199–210.

396 Chen, Y., Oliver, D. S., et al. (2010). “Parameterization techniques to improve mass conservation
397 and data assimilation for ensemble kalman filter.” *SPE Western Regional Meeting*, Society of
398 Petroleum Engineers.

399 Chen, Z., Gómez-Hernández, J. J., Xu, T., and Zanini, A. (2018). “Joint identification of contam-
400 inant source and aquifer geometry in a sandbox experiment with the restart ensemble kalman
401 filter.” *Journal of hydrology*, 564, 1074–1084.

402 de Marsily, G., Lavedan, G., Boucher, M., and FASAMINO, G. (1984). “Interpretation of inter-
403 ference tests in a well field using geostatistical techniques to fit the permeability distribution in
404 a reservoir model.” *Geostatistics for natural resources characterization. NATO advanced Study*
405 *Institute*, 831–849.

406 De Sanctis, A. E., Shang, F., and Uber, J. G. (2010). “Real-time identification of possible contami-
407 nation sources using network backtracking methods.” *Journal of Water Resources Planning and*
408 *Management*, 136(4), 444–453.

409 D’Oria, M., Ferrari, A., Mignosa, P., Tanda, M. G., and Vacondio, R. (2017). “Reverse flow routing
410 in a bayesian framework using a gpu-accelerated 2d shallow water model.” *AGUFM*, 2017,
411 H11E–1218.

412 D’Oria, M., Mignosa, P., and Tanda, M. G. (2014). “Bayesian estimation of inflow hydrographs in
413 ungauged sites of multiple reach systems.” *Advances in water resources*, 63, 143–151.

414 Eliades, D. G. and Polycarpou, M. M. (2012). “Water contamination impact evaluation and source-
415 area isolation using decision trees.” *Journal of Water Resources Planning and Management*,
416 138(5), 562–570.

417 Evensen, G. (1994). “Sequential data assimilation with a nonlinear quasi-geostrophic model using
418 Monte Carlo methods to forecast error statistics.” *Journal of Geophysical Research*, 99(C5),
419 10143.

420 Evensen, G. (2003). “The Ensemble Kalman Filter: Theoretical formulation and practical imple-
421 mentation.” *Ocean Dynamics*, 53(4), 343–367.

422 Franssen, H. H. and Kinzelbach, W. (2009). “Ensemble kalman filtering versus sequential self-
423 calibration for inverse modelling of dynamic groundwater flow systems.” *Journal of Hydrology*,
424 365(3-4), 261–274.

425 Hart, W. E. and Murray, R. (2010). “Review of sensor placement strategies for contamination
426 warning systems in drinking water distribution systems.” *Journal of Water Resources Planning
427 and Management*, 136(6), 611–619.

428 Kim, M., Choi, C. Y., and Gerba, C. P. (2008). “Source tracking of microbial intrusion in water
429 systems using artificial neural networks.” *Water research*, 42(4-5), 1308–1314.

430 Koch, J. and Nowak, W. (2016). “Identification of contaminant source architectures - A statistical
431 inversion that emulates multiphase physics in a computationally practicable manner.” *Water
432 Resources Research*, 52(2), 1009–1025.

433 Li, L., Zhou, H., Hendricks Franssen, H.-J., and Gómez-Hernández, J. J. (2012). “Modeling tran-
434 sient groundwater flow by coupling ensemble kalman filtering and upscaling.” *Water Resources
435 Research*, 48(1).

436 Liu, L., Ranjithan, S. R., and Mahinthakumar, G. (2011). “Contamination source identification in
437 water distribution systems using an adaptive dynamic optimization procedure.” *Journal of Water
438 Resources Planning and Management*, 137(2), 183–192.

439 Liu, L., Zechman, E. M., Mahinthakumar, G., and Ranji Ranjithan, S. (2012). “Identifying con-
440 taminant sources for water distribution systems using a hybrid method.” *Civil Engineering and*
441 *Environmental Systems*, 29(2), 123–136.

442 Michalak, A. M. and Kitanidis, P. K. (2004). “Estimation of historical groundwater contaminant
443 distribution using the adjoint state method applied to geostatistical inverse modeling.” *Water*
444 *Resources Research*, 40(8).

445 Neupauer, R. M. and Wilson, J. L. (1999). “Adjoint method for obtaining backward-in-time location
446 and travel time probabilities of a conservative groundwater contaminant.” *Water Resources*
447 *Research*, 35(11), 3389–3398.

448 Perelman, L. and Ostfeld, A. (2013). “Bayesian networks for source intrusion detection.” *Journal*
449 *of Water Resources Planning and Management*, 139(4), 426–432.

450 Rajakumar, A. G., Mohan Kumar, M., Amrutur, B., and Kapelan, Z. (2019). “Real-time water qual-
451 ity modeling with ensemble kalman filter for state and parameter estimation in water distribution
452 networks.” *Journal of Water Resources Planning and Management*, 145(11), 04019049.

453 Rossman, L. A. (2000). “Epanet 2: users manual.

454 Schöniger, A., Nowak, W., and Hendricks Franssen, H.-J. (2012). “Parameter estimation by ensem-
455 ble kalman filters with transformed data: Approach and application to hydraulic tomography.”
456 *Water Resources Research*, 48(4).

457 Seth, A., Klise, K. A., Sirola, J. D., Haxton, T., and Laird, C. D. (2016). “Testing contamination
458 source identification methods for water distribution networks.” *Journal of Water Resources*
459 *Planning and Management*, 142(4), 04016001.

460 Shen, H. and McBean, E. (2012). “False negative/positive issues in contaminant source identifi-
461 cation for water-distribution systems.” *Journal of Water Resources Planning and Management*,
462 138(3), 230–236.

463 Sun, A. Y., Morris, A. P., and Mohanty, S. (2009). “Sequential updating of multimodal hydrogeo-
464 logic parameter fields using localization and clustering techniques.” *Water Resources Research*,
465 45(7).

466 Sun, A. Y., Painter, S. L., and Wittmeyer, G. W. (2006). “A constrained robust least squares approach
467 for contaminant release history identification.” *Water Resources Research*, 42(4), 1–13.

468 Todaro, V., D’Oria, M., Tanda, M. G., and Gómez-Hernández, J. J. (2019). “Ensemble smoother
469 with multiple data assimilation for reverse flow routing.” *Computers & Geosciences*, 131, 32–40.

470 Tryby, M. E., Propato, M., and Ranjithan, S. R. (2010). “Monitoring design for source identification
471 in water distribution systems.” *Journal of Water Resources Planning and Management*, 136(6),
472 637–646.

473 Ung, H., Piller, O., Gilbert, D., and Mortazavi, I. (2017). “Accurate and optimal sensor placement
474 for source identification of water distribution networks.” *Journal of Water Resources Planning
475 and Management*, 143(8), 04017032.

476 Walski, T. M., Brill Jr, E. D., Gessler, J., Goulter, I. C., Jeppson, R. M., Lansey, K., Lee, H.-L.,
477 Liebman, J. C., Mays, L., Morgan, D. R., et al. (1987). “Battle of the network models: Epilogue.”
478 *Journal of Water Resources Planning and Management*, 113(2), 191–203.

479 Wang, H. and Harrison, K. W. (2013). “Bayesian update method for contaminant source character-
480 ization in water distribution systems.” *Journal of Water Resources Planning and Management*,
481 139(1), 13–22.

482 Wang, H. and Harrison, K. W. (2014). “Improving efficiency of the bayesian approach to water
483 distribution contaminant source characterization with support vector regression.” *Journal of
484 Water Resources Planning and Management*, 140(1), 3–11.

485 Wen, X.-H., Capilla, J. E., Deutsch, C., Gómez-Hernández, J., and Cullick, A. (1999). “A program
486 to create permeability fields that honor single-phase flow rate and pressure data.” *Computers &
487 Geosciences*, 25(3), 217–230.

488 Woodbury, A. D. and Ulrych, T. J. (1993). “Minimum relative entropy: Forward probabilistic
489 modeling.” *Water Resources Research*, 29(8), 2847–2860.

490 Woodbury, A. D. and Ulrych, T. J. (1996). “Minimum relative entropy inversion: Theory and
491 application to recovering the release history of a groundwater contaminant.” *Water Resources
492 Research*, 32(9), 2671–2681.

493 Xu, T. and Gómez-Hernández, J. J. (2016). “Joint identification of contaminant source location,
494 initial release time, and initial solute concentration in an aquifer via ensemble Kalman filtering.”
495 *Water Resources Research*.

496 Xu, T. and Gómez-Hernández, J. J. (2018). “Simultaneous identification of a contaminant source
497 and hydraulic conductivity via the restart normal-score ensemble Kalman filter.” *Advances in*
498 *Water Resources*, 112(July 2017), 106–123.

499 Xu, T., Gómez-Hernández, J. J., Zhou, H., and Li, L. (2013). “The power of transient piezometric
500 head data in inverse modeling: An application of the localized normal-score enkf with covariance
501 inflation in a heterogenous bimodal hydraulic conductivity field.” *Advances in water resources*,
502 54, 100–118.

503 Yang, X. and Boccelli, D. L. (2014). “Bayesian approach for real-time probabilistic contami-
504 nation source identification.” *Journal of Water Resources Planning and Management*, 140(8),
505 04014019.

506 Ye, G. and Fenner, R. A. (2014). “Study of burst alarming and data sampling frequency in water dis-
507 tribution networks.” *Journal of Water Resources Planning and Management*, 140(6), 06014001.

508 Zhou, H., Gómez-Hernández, J. J., and Li, L. (2014). “Inverse methods in hydrogeology: Evolution
509 and recent trends.” *Advances in Water Resources*, 63, 22–37.

510 Zhou, H., Li, L., Franssen, H.-J. H., and Gómez-Hernández, J. J. (2012). “Pattern recognition in
511 a bimodal aquifer using the normal-score ensemble kalman filter.” *Mathematical Geosciences*,
512 44(2), 169–185.

513 **List of Tables**

514 1 Scenarios considered 22

515 2 Indicators 23

TABLE 1. Scenarios considered

Scenario	Source location node number	Source intensity mg l ⁻¹	t_1 min	t_{max} min	Δt min
S1	1	100	180	360	10
S2	2	100	60	300	30
S3	3	100	180	430	10
S4	4	100	60	300	30
S5	8	100	180	600	10
S6	9	100	180	600	30
S7	10	100	180	600	10
S8	11	100	180	600	10
S9	12	100	60	390	30
S10	13	100	60	360	30
S11	14	100	180	600	10
S12	15	100	60	390	30
S13	16	100	180	600	10
S14	17	100	180	600	10
S15	18	100	60	200	10
S16	19	100	60	300	30

TABLE 2. Indicators

Scenario	$i_1(t_{max})$ $\cdot 10^{-2}$	$i_2(t_{max})$ $\cdot 10^{-2}$	$i_3(t_{max})$ $\cdot 10^{-2}$	$i_4(t_{max})$ $\cdot 10^{-2}$	Average distance from source location in m at t_{max}	Average difference from true intensity in mg l^{-1} at t_{max}
S1	0.00	0.00	0.04	0.43	0.00	-0.43
S2	2.90	1.76	2.94	5.03	16.23	4.02
S3	0.27	1.73	1.82	4.25	18.62	3.82
S4	0.92	1.74	4.84	6.96	16.33	-5.27
S5	0.00	4.15	5.05	7.87	36.38	5.83
S6	4.77	3.39	7.00	9.12	40.95	-6.41
S7	0.00	0.00	0.00	0.13	0.00	3.46
S8	1.83	15.74	5.58	0.32	148.00	-6.34
S9	0.00	8.86	3.38	0.23	69.16	4.73
S10	0.84	0.40	1.67	1.65	2.88	0.10
S11	1.21	0.74	0.96	1.93	5.18	-1.69
S12	1.75	3.14	5.71	6.33	21.41	2.55
S13	0.11	7.23	1.59	12.85	47.35	12.73
S14	0.00	3.04	1.86	1.87	25.18	-0.35
S15	0.00	18.93	2.17	2.90	117.38	-1.99
S16	1.82	20.17	5.72	7.54	118.16	4.67

516
517
518
519
520
521
522
523
524
525
526
527
528
529
530
531

List of Figures

1	Sketch of the Anytown WDS, (a) original, (b) with all pipes discretized, and (c) with an indication of the ensemble of 48 initial release locations.	25
2	Histograms of indicators i_1 (coordinate spread) and i_2 (coordinate bias) for all scenarios at $t = t_{max}$	26
3	Histograms of indicators i_3 (intensity spread) and i_4 (intensity bias) for all scenarios at $t = t_{max}$	27
4	Scenario 6. (a) Time evolution of i_1 and i_2 . (b) Spatial distribution of the source estimate positions of all 48 realizations at time t_{max} (light squares).	28
5	Scenario 12. (a) Time evolution of i_1 and i_2 . (b) Spatial distribution of the source estimate positions of all 48 realizations at time t_{max} (light squares).	29
6	Time evolution of i_3 and i_4 for scenarios 6 and 12.	30
7	Time evolution of the ensemble of source locations. Source positions shown by light squares.	31
8	Time evolution of the ensemble of source locations. Source positions shown by light squares.	32

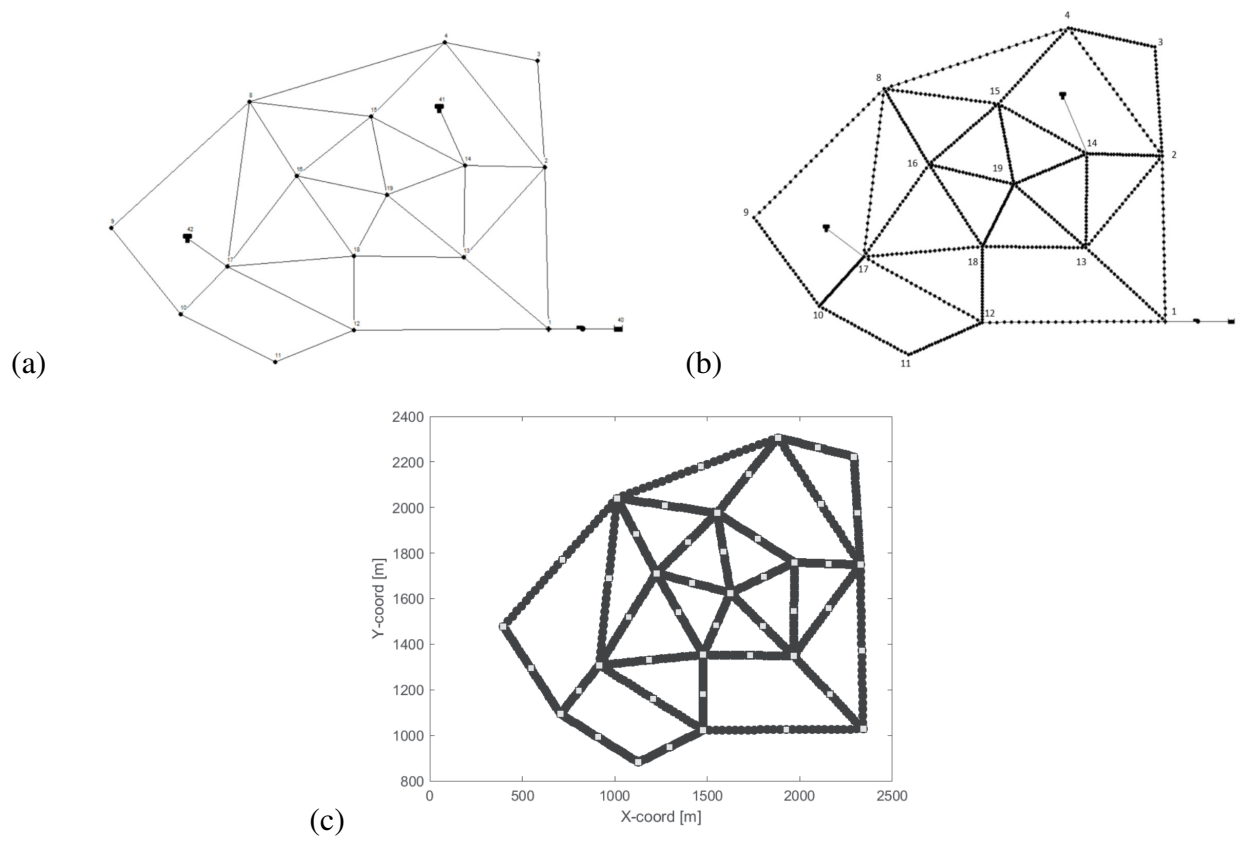


Fig. 1. Sketch of the Anytown WDS, (a) original, (b) with all pipes discretized, and (c) with an indication of the ensemble of 48 initial release locations.

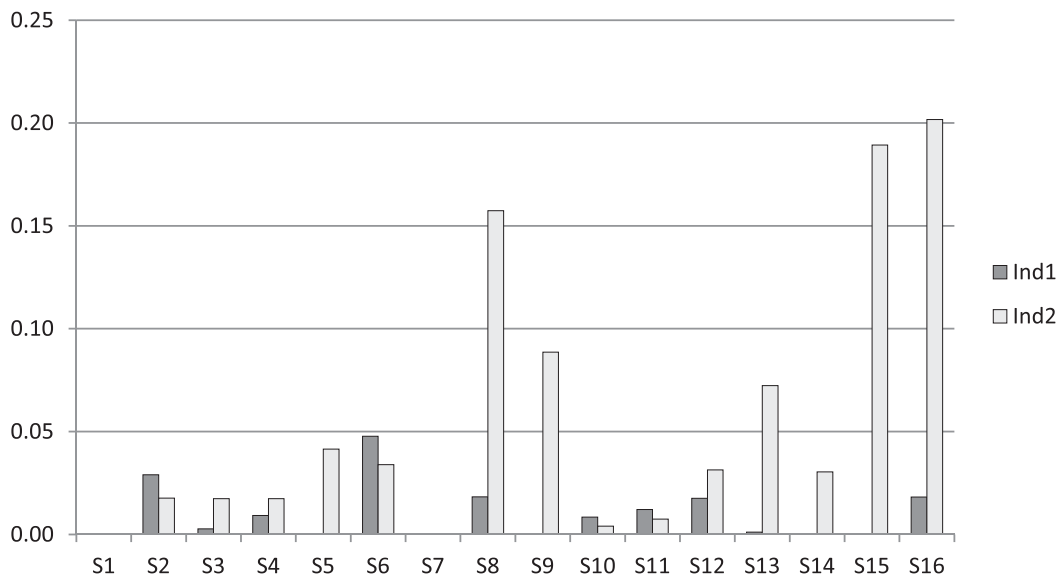


Fig. 2. Histograms of indicators i_1 (coordinate spread) and i_2 (coordinate bias) for all scenarios at $t = t_{max}$.

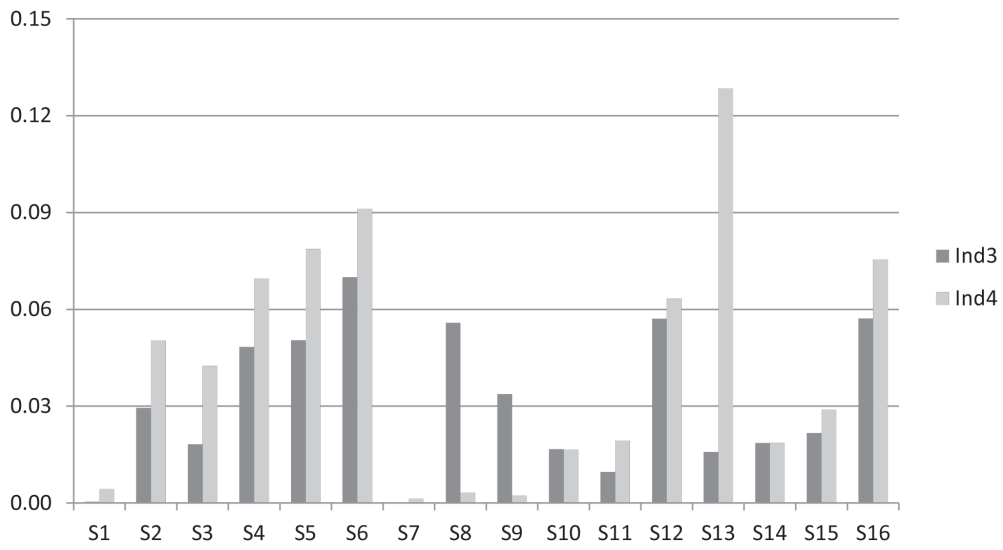


Fig. 3. Histograms of indicators i_3 (intensity spread) and i_4 (intensity bias) for all scenarios at $t = t_{max}$.

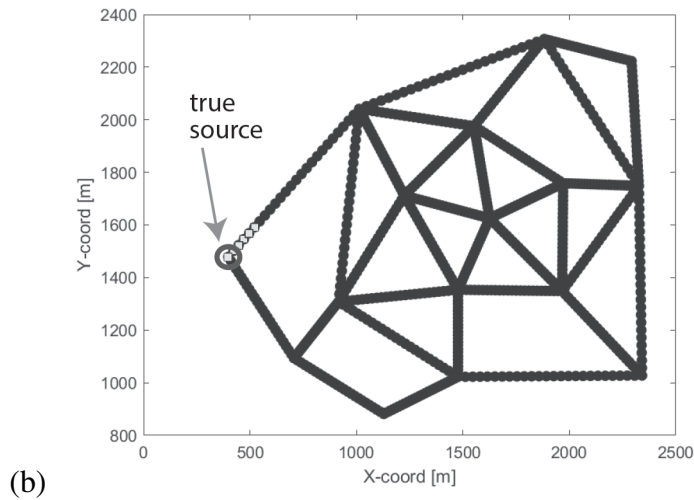
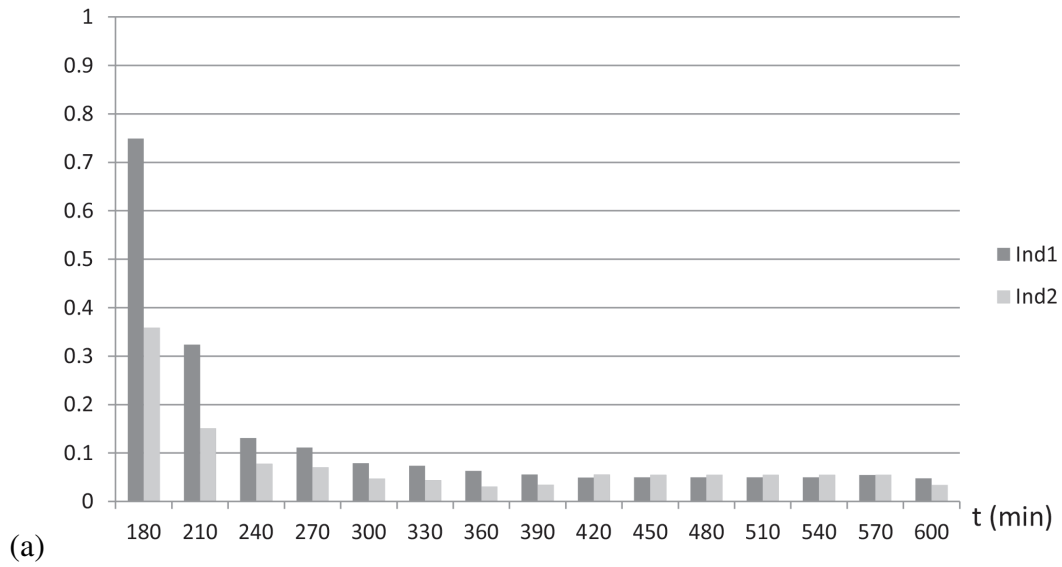


Fig. 4. Scenario 6. (a) Time evolution of i_1 and i_2 . (b) Spatial distribution of the source estimate positions of all 48 realizations at time t_{max} (light squares).

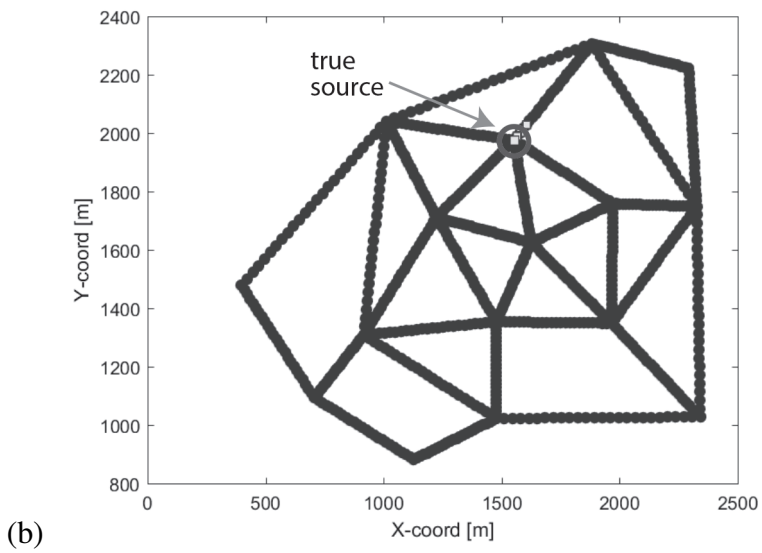
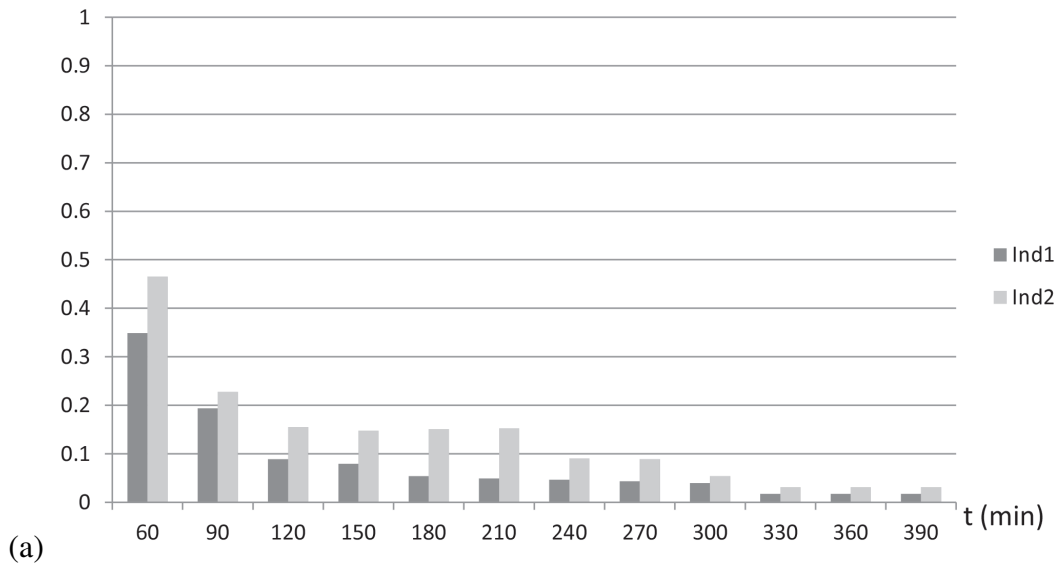


Fig. 5. Scenario 12. (a) Time evolution of i_1 and i_2 . (b) Spatial distribution of the source estimate positions of all 48 realizations at time t_{max} (light squares).

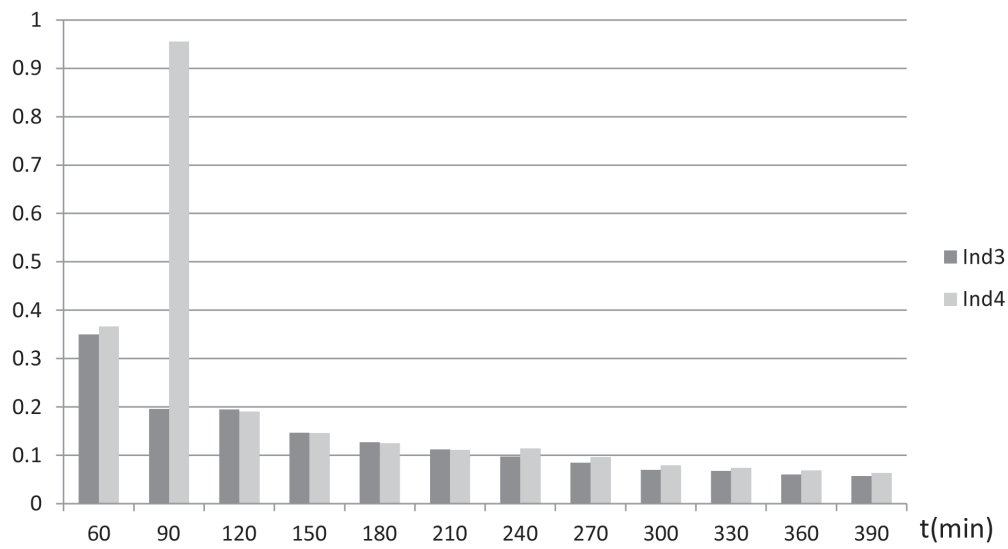
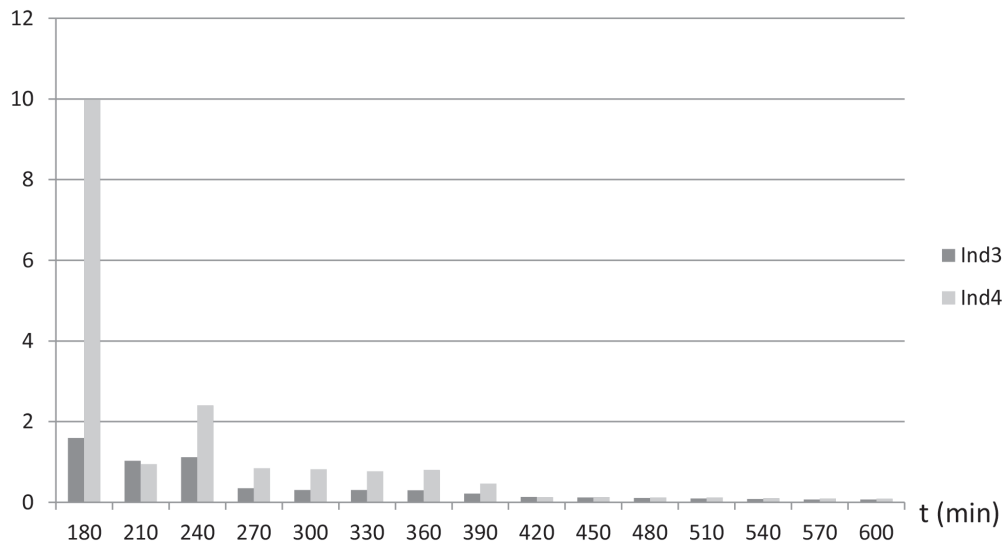


Fig. 6. Time evolution of i_3 and i_4 for scenarios 6 and 12.

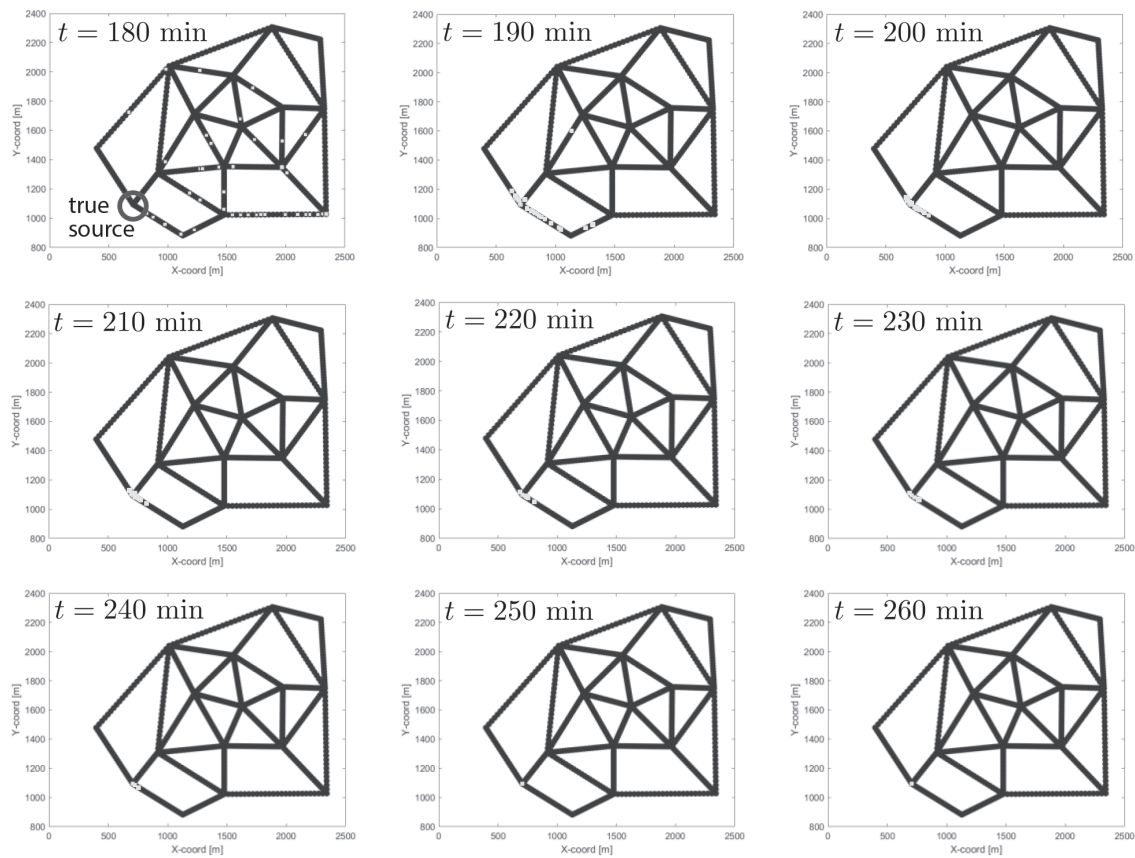


Fig. 7. Time evolution of the ensemble of source locations. Source positions shown by light squares.

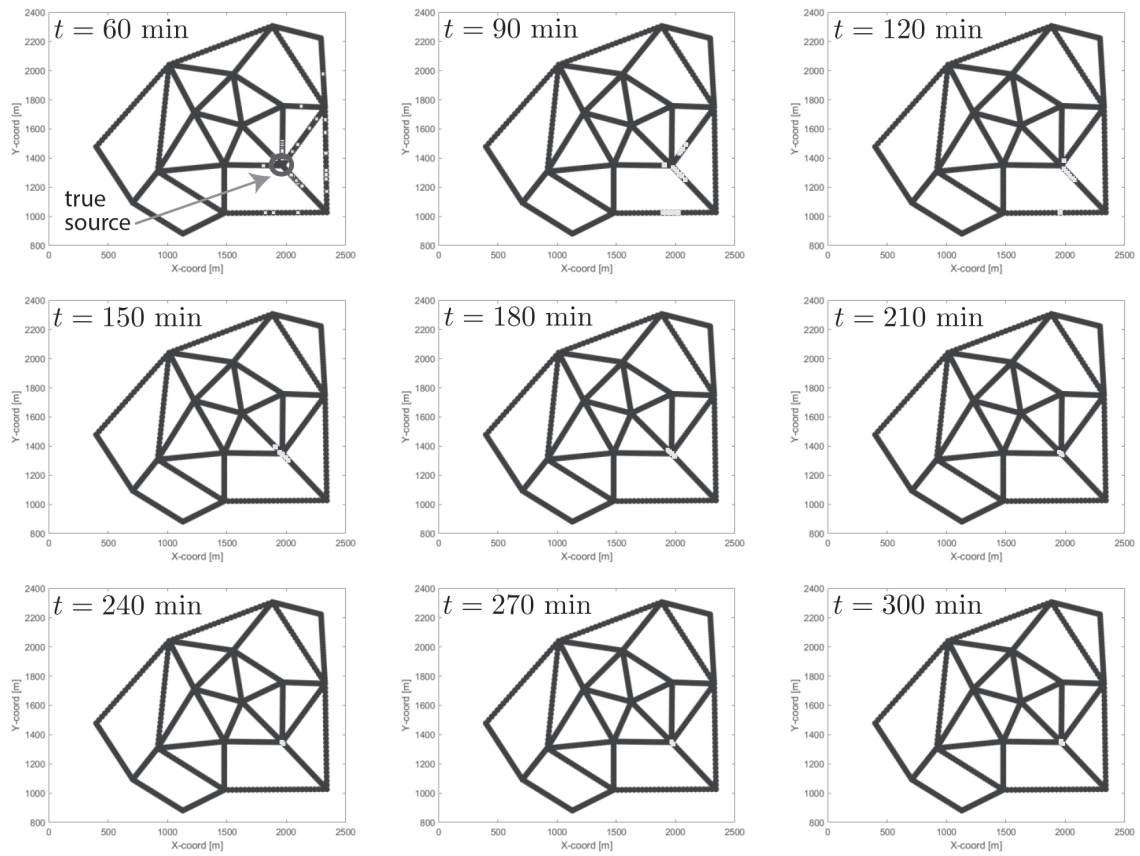


Fig. 8. Time evolution of the ensemble of source locations. Source positions shown by light squares.